An extension of dynamic droplet deformation models to secondary atomization

F.-O. Bartz*, R. Schmehl†, R. Koch and H.-J. Bauer
Institut für Thermische Strömungsmaschinen
Karlsruher Institut für Technologie (KIT)
Karlsruhe, Germany
†Faculty of Aerospace Engineering
Delft University of Technology
Delft, The Netherlands

Abstract

A detailed model for secondary atomization of liquid droplets by aerodynamic forces is presented. As an empirical extension of dynamic droplet deformation models, it accounts for temporal variations of the relative velocity between droplet and gas phase during the deformation and breakup process and describes the characteristic features of different breakup mechanisms (deformation kinetics, aerodynamics and product properties). Computed droplet trajectories and Sauter mean diameters have been compared using the proposed deformation-based model and a model using a breakup criterion based on the local instantaneous Weber number. It is concluded, that a deformation-based criterion should be used for droplets exposed to complex aerodynamic loading and that more experimental research is required to identify the accuracy of the presented detailed breakup product model.

Introduction

Fuel preparation for combustion applications is often characterized by a strong interaction of the spray with a complex gas flow field. The gas phase velocity field is generally unsteady, with distinctive three-dimensional velocity gradients. Consequently, the droplets are subjected to a spectrum of relative velocity fluctuations. When these exceed a certain intensity, deformation and secondary breakup begin to occur. Droplet breakup is governed by several distinctive mechanisms - bag, multimode and shear breakup according to the terminology of Hsiang and Faeth [12]-, depending on the intensity of the aerodynamic forces.

In many application scenarios, the time scale of deformation and breakup is comparable to or larger than the characteristic scales of the gas flow fluctuations, i.e. the relative velocity varies significantly during the deformation and breakup process. In these cases, the deformation and breakup process and, consequently, the characteristics of secondary fragments do not depend only on instantaneous local flow situations but on the variation of aerodynamic forces during the disintegration process. Figure 1 illustrates the temporal evolution of the aerodynamic loading of droplets for some example applications. The time scale, T, is normalized by the characteristic time of free shape oscillations

$$t_\sigma^* = \sqrt{\frac{D_0^3\,\rho_d}{\sigma}}\,. \tag{1}$$

It is obvious that in complex flow fields, e.g. in a premixing module of a combustor, the aerodynamic loading differs significantly from the loading in a shocktube. Secondary atomization models which do not take into account these relative velocity fluctuations may incorrectly predict the resulting droplet trajectories, sizes and velocities.

In this paper, a breakup model for the use in a Lagrange-particle tracking code is proposed. Common secondary breakup models implemented in commercial or opensource CFD-codes are the Taylor Analogy Breakup model (TAB) [19], the Enhanced TAB-model [29], the Reitz and Diwakar breakup model [22], the wave breakup model [23] as well as the semi-empirical Schmehl [24] breakup model. The proposed model takes into account the temporal evolution of the aerodynamic loading of the droplet. A critical deformation is used as breakup criterion. The actual disintegration process is described empirically. Secondary droplet properties are computed either by global statistical or by detailed deterministic correlations.

Breakup model

Prior to the description of the breakup model a short introduction of the breakup process is given. The temporal evolution of droplet deformation and breakup is depicted in Figure 2 for impulsive aerodynamic loading. The

*Corresponding author: frank-oliver.bartz@kit.edu

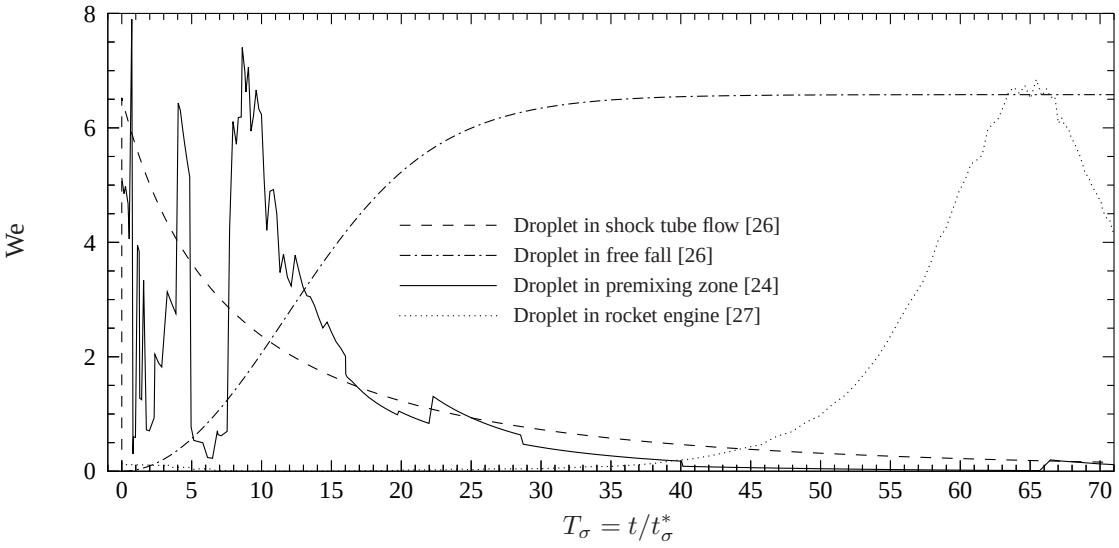

Figure 1. Scenarios of aerodynamic loading [26]

experimental data typically implies, that the relative velocity remains approximately constant during the disintegration process. The non-dimensional time, T, is defined as the ratio of the time, t, and the characteristic deformation time

$$t^* = \sqrt{\frac{\rho_d}{\rho_g}} \frac{D_0}{v_{rel}} \,. \tag{2}$$

The stages of droplet deformation and breakup are defined by the non-dimensional characteristic times when the disc-shaped droplet reaches its minimal thickness T_{min}, the start of the breakup process T_i and the end of the breakup process T_b. The transitions are functions of the Weber and Ohnesorge number. The regions where liquid is actually disintegrating are marked by shading. The dashed line illustrates the correlation for T_b proposed by Pilch and Erdman [21].

Common for all breakup regimes is, as illustrated in Figure 2, that the droplet flattens during an initial phase. For bag breakup, a thin, bag-shaped film pocket is formed, which then disintegrates into many tiny drops. Afterwards, the ring disintegrates by a Rayleigh-like breakup process into larger fragments. In the bag-plume breakup regime, a concentric bag forms first, suspended from a plume column at the center. The bag disintegrates first, followed by the ring, and later, detachment of a core droplet from the plume occurs according to Dai and Faeth [4]. Finally, the plume droplet disintegrates. At increased Weber numbers, the core drop forms after the plume undergoes breakup. The core drop then undergoes Rayleigh-type breakup. In the plume-shear breakup regime, a plume forms, with the core droplet attached to the plume [4]. Small fragments are continuously separated from the plume-core droplet complex. The plume-core droplet complex disintegrates relatively slowly. In the shear breakup regime, small fragments are separated from the droplet equator until a stable diameter of the core droplet is left. Guildenbecher et al. [9] state that the shear stripping model used by Chou and Faeth [2] is incorrect, and that this breakup regime is the result of sheet-thinning. This has also been proposed by Liu and Reitz [18]. The results obtained by Chou and Faeth [2] can be explained using the sheet-thinning mechanism.

The proposed droplet breakup model combines a dynamic deformation model and an empirical description of the breakup process. The mechanistic deformation model is based on one or more ordinary differential equations describing the evolution of the droplet shape as a result of the aerodynamic forces. Therefore, differential equations for the deformation state are numerically integrated, similar to the droplet motion and other physical processes such as droplet evaporation. The initial phase of transverse distortion and flattening of the droplet is computed using the deformation model. Once a critical deformation is reached, the breakup process is prescribed on the basis of a semi-empirical model. This model is based on experimental data obtained by shock-loading the droplet.

Since the aerodynamic loading of the droplet is variable, a fictive onset of shock-loading conditions is predicted. This prediction is performed at the latest stage computed by the dynamic droplet deformation model to account for the variation of the aerodynamic loading as long as possible. The classification of the breakup regime is performed when the drop reaches its critical deformation. The approximation of the characteristic times is evaluated when the droplet reaches its maximum deformation which is resolved by the deformation model.

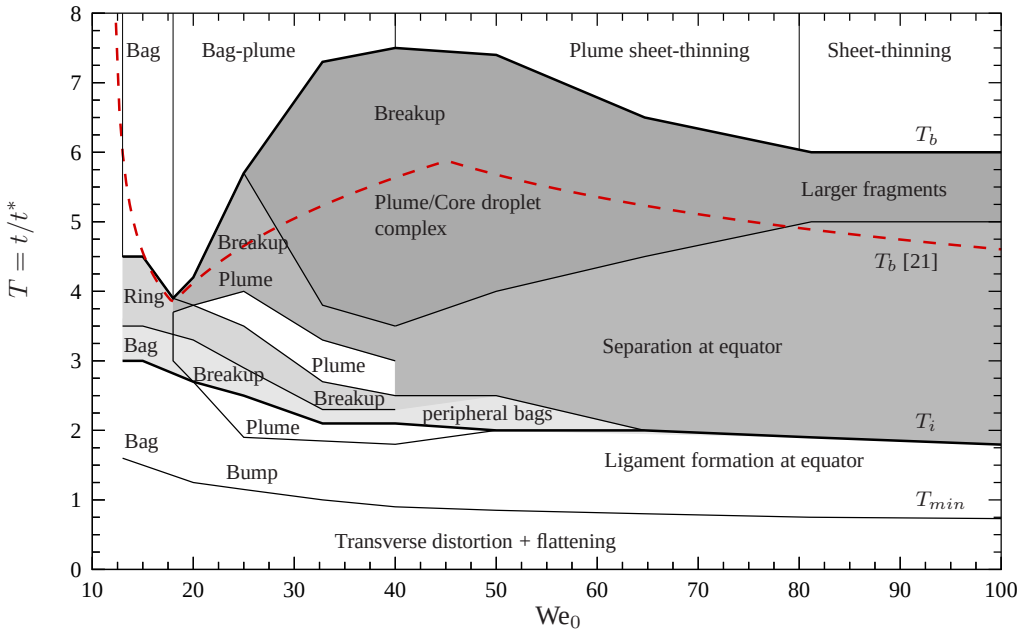

Figure 2. Temporal evolution of droplet deformation and breakup for impulsive aerodynamic loading, experimental data base from [4], [15] and [30]. Figure adapted from [26].

Droplet deformation

Subcritical deformations as well as the initial deformation phase during breakup can be computed by the Normal-Mode model (NM) and Non-linear Taylor Analogy Breakup model (NLTAB) as described by Schmehl [25, 26]. The NLTAB-model is a nonlinear variant of the TAB-model [19] and is based on the experimental observation that the droplet deformation in air flows can be represented by spheroidal (oblate and prolate) shapes. The NM-model is based on linear Normal Mode analysis and is capable to describe arbitrary shape variations in the limit of small amplitudes. In the current approach, the NLTAB model is used, since large deformations of the droplet are expected which cannot accurately be described by a linear model [26]. The NLTAB-model describes the droplet deformation dynamics in terms of the non-dimensional equator coordinate y, which is defined as the ratio of the cross-stream diameter to the spherical diameter $y = D/D_0$. The aerodynamic drag coefficient c_D of the droplet is determined from a linear interpolation between the drag coefficient of a spherical drop and a disc-shaped drop, $c_D = f\, c_{D,sphere} + (1 - f)\, c_{D,disc}$. The interpolation is based on the variable $f = 1 - E^2$, with E being the aspect ratio of the droplet defined as $E = 1/y^3$ [25].

Critical deformation and deformation during the breakup process

The deformation and breakup processes occurring for $T > T_{min}$ cannot be described using the dynamic droplet deformation model. For this phase, an empirical description of these processes is proposed.

In the current approach, deformation is resolved using the dynamic deformation models until a maximum non-dimensional coordinate y_{max} is reached. Schmehl [26] performed calculations of the maximum non-dimensional equator coordinate for shock-loaded droplets for $On < 0.1$ using the NLTAB-model. At the onset of bag breakup for a critical Weber number of $We_{0,c} = 13$ he obtained a maximum deformation of

$$y_c \approx 1.8\,. \tag{3}$$

Experimental data from Kim [13] confirm this critical deformation. Aalburg et. al. [1] performed direct numerical simulations of shock-loaded droplets. They concluded that the critical deformation noted in Equation (3) is an excellent estimate of the critical deformation at the onset of breakup for a large range of Ohnesorge numbers.

For higher We, the maximum non-dimensional coordinate reaches higher amplitudes before breakup. By analyzing experimental data for shock-loading conditions published by Dai and Faeth [4], it can be concluded that the maximum non-dimensional coordinate of disintegrating droplets reaches a maximum amplitude

$$y_{max} \approx 2.1\,, \qquad \text{for } We_0 > 20. \tag{4}$$

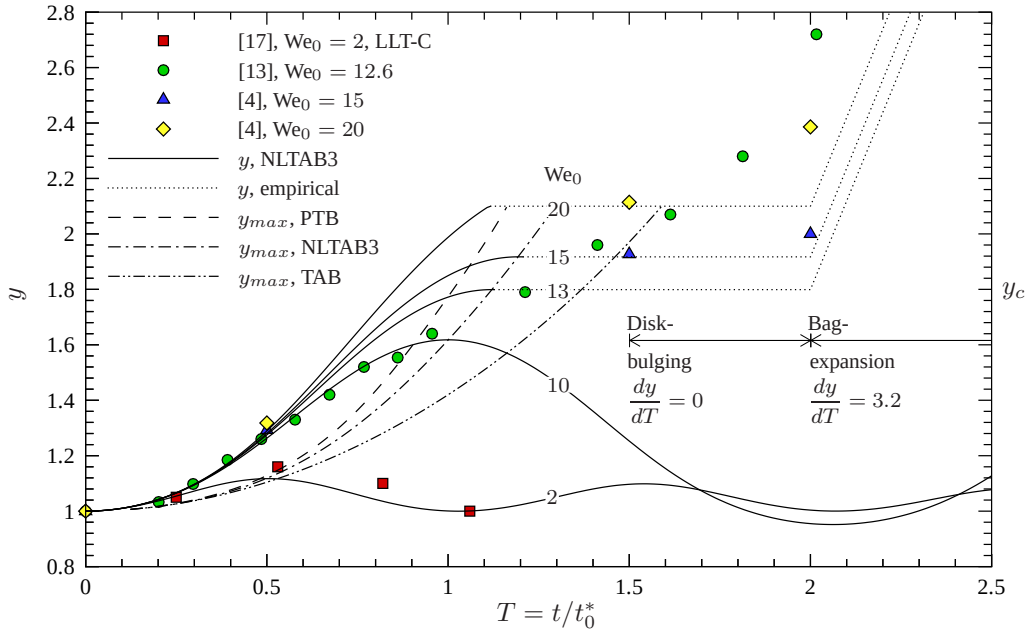

Figure 3. Droplet transverse deformation from shock loading [26]

The suggested modeling approach is illustrated in Figure 3. Droplet deformation is modeled by the NLTAB-model until either the non-dimensional deformation exceeds the critical deformation y_c and the first derivative of the non-dimensional equator coordinate after the time reaches zero, $dy/dt = 0$, or the maximal non-dimensional deformation $y_{max} = 2.1$ is reached.

After the droplet reaches its maximum non-dimensional coordinate ($1.8 \leq y_{max} \leq 2.1$) the breakup process is initiated, which is described empirically. During the bulging of the disc (until $T = 2$), it is assumed that the cross-stream dimension of the droplet remains constant. Then, during bag expansion, the development of the non-dimensional coordinate is described by the following equation, which Schmehl [26] obtained by analyzing data of Dai and Faeth [4]

$$\frac{dy}{dT} \approx 3.2\,, \qquad \text{for } T > 2\,. \tag{5}$$

This linear size increase continues until the breakup process is terminated. This universal value can also be obtained by analyzing experimental data of Kim [13], Krzeczkowski [15], Lane [16] and Gutknecht [10] and is independent of the actual breakup mechanism for We$_0 \leq 100$.

Identification of breakup regime

In the suggested approach the breakup regime is identified when the droplet reaches its critical deformation. The objective is to account for possible temporal variations of the aerodynamic loading as long as possible. The breakup regime is identified using the instantaneous Weber number when the critical non-dimensional coordinate y_c is reached.

Since no comprehensive experimental study with reported transition Weber numbers at the critical deformation is available, numerical simulations have been used to derive these numbers. Therefore, simulations with the NLTAB-model have been performed by Schmehl [26]. He simulated the deformation of droplets at shock loading conditions with initial Weber numbers We$_0$ which are listed in Table 1. These Weber numbers were obtained as transition values between breakup regimes from Hsiang and Faeth [12] and Dai and Faeth [4]. The Ohnesorge number and Weber number were varied by altering the liquid viscosity μ_d and the relative velocity v_{rel}. The parameters $D_0, \rho_g, \mu_g, \rho_d$ and σ have been adopted from Hsiang and Faeth [12]. The acceleration of the droplet is accounted for by an acceleration corrected drag coefficient $c_D = c_{D,\infty} - (\rho_d/\rho - 1)\,/A_c$, where $A_c = \left(D/v_{rel}^2\, dv_{rel}/dt\right)^{-1}$. The corresponding Weber numbers when the droplet reaches $y_c = 1.8$ are listed in Table 1.

Table 1. Identification of breakup regime [26]

breakup regime	bag-plume	multi-mode	plume-shear	shear
$\mathrm{We}\vert_{y_c}$	11.5	27	32	64
We_0 for $\mathrm{On} << \mathrm{On}_c$	18	35	40	80

Onset of semi-empirical modeling

As mentioned before, experimental data used to describe the breakup process are from experiments in a shock tube. Since the aerodynamic loading of droplets in complex systems deviates strongly from shock-loading conditions, the non-dimensional time, $T = t/t_0^*$, and the initial Weber number for shock-loading conditions, We_0, are predicted when the droplet reaches its maximum deformation y_{max}.

Since no experimental correlations to obtain We_0 and T_{ymax} when y_{max} is reached are known, correlations have been developed using numerical simulations. The NLTAB-model has been used to describe the deformation of droplets exposed to shock-loading conditions. The Weber number, Ohnesorge number and Reynolds number were varied by altering v_{rel}, μ_d and μ_g, while the following parameters were held fix: $D_0 = 50\mu m$, $\rho_g = 1.2\, kg/m^3$, $\rho_d = 997.2\, kg/m^3$ and $\sigma = 0.02037\, N/m$. The Ohnesorge number was varied from $0.0005 < \mathrm{On} < 0.15$, the Weber number from $= 11 < \mathrm{We} < 80$ and the Reynolds number at initial conditions was varied from $= 36 < Re < 3955$. The Reynolds number at the maximum deformation $\mathrm{Re}_{ymax} = \rho_g\, v_{rel}\, D/\mu_g$ is calculated using the cross stream diameter D to account for the drag, whereas the Weber number and the Ohnesorge number are computed using the volume equivalent diameter. Following equations describe the best fit of the evaluated data:

$$\mathrm{We}_0 = \begin{cases} 1.0525\, \mathrm{We}_{ymax}^{1.0195}\, \mathrm{Re}_{ymax}^{-0.01069}\, \mathrm{On}^{0.0024} + 1.6056, & \text{for} \quad y_{max} = 2.1 \\ 1.0964\, \mathrm{We}_{ymax}^{1.0894}\, \mathrm{Re}_{ymax}^{-0.02224}\, \mathrm{On}^{-0.004318} - 1.1291, & \text{for} \quad y_{max} < 2.1 \end{cases} \tag{6}$$

$$T_{ymax} = \begin{cases} 94.5718\, \mathrm{We}_{ymax}^{-1.7147}\, \mathrm{Re}_{ymax}^{0.001826}\, \mathrm{On}^{0.2481} + 0.82475, & \text{for} \quad y_{max} = 2.1 \\ 0.07803\, \mathrm{We}_{ymax}^{0.8899}\, \mathrm{Re}_{ymax}^{-0.005996}\, \mathrm{On}^{-0.001373} + 0.4566, & \text{for} \quad y_{max} < 2.1 \end{cases} \tag{7}$$

An application of Equation (7) to the data used to derive this equation yields mean relative errors of 0.6 % for $y_{max} = 2.1$ and 0.8% for $y_{max} < 2.1$. For Equation (7) the corresponding mean relative errors are 2.1% and 0.5% respectively. A comparison of this data to validation data that was also generated by the NLTAB-model for $12 < \mathrm{We}_0 < 125$, $0.001 < \mathrm{On} < 0.1$ and $36 < \mathrm{Re} < 3955$ yielded mean relative errors of 7.2% and 13.8% for Equation (6) and 1.8% as well as 4.4% for Equation (7).

To calculate the relative time based on shock-loading conditions $t_{y,max,rel} = T_{y,max}\, t_0^*$ and the time for the fictive start of the shock-loading conditions $t_{start} = t - t_{ymax,rel}$, the characteristic deformation time t_0^* has to be calculated. The characteristic time of free shape oscillations t_σ^* is calculated according to Equation (1) when the droplet reaches its maximum deformation y_{max}. It is assumed that t_σ^* is much smaller than the characteristic time scale of evaporation, so the diameter decrease in the time period between the assumed shock loading conditions and the droplet reaching y_{max} is insignificant. The rate of change of the density and surface tension is also assumed to be negligible. The characteristic deformation time is then linked to the characteristic time of free shape oscillations by $t_0^* = t_\sigma^* / \left(\mathrm{We}_0\right)^{0.5}$.

Figure 4 displays the temporal placement of the relevant times used in this model, with $t_{db} = t_{start} + 2\, t_0^*$ being the time when bulging of the disc is completed. As mentioned before, a constant non-dimensional coordinate $y = y_{max}$ is assumed for $t_{ymax} < t < t_{db}$. The time when the secondary droplets are generated is termed t_{break}.

Breakup times

The following correlations for the end of breakup time t_b are suggested by Pilch and Erdman [21] for low Ohnesorge numbers $On < 0.1$:

$$\frac{t_b}{t_0^*} = \begin{cases} 6\left(\mathrm{We}_0 - 12\right)^{-0.25}, & \text{for} \quad 12 < \mathrm{We}_0 < 18 \\ 2.45\left(\mathrm{We}_0 - 12\right)^{0.25}, & \text{for} \quad 18 < \mathrm{We}_0 < 45 \\ 14.1\left(\mathrm{We}_0 - 12\right)^{-0.25}, & \text{for} \quad 45 < \mathrm{We}_0 < 351 \end{cases} \tag{8}$$

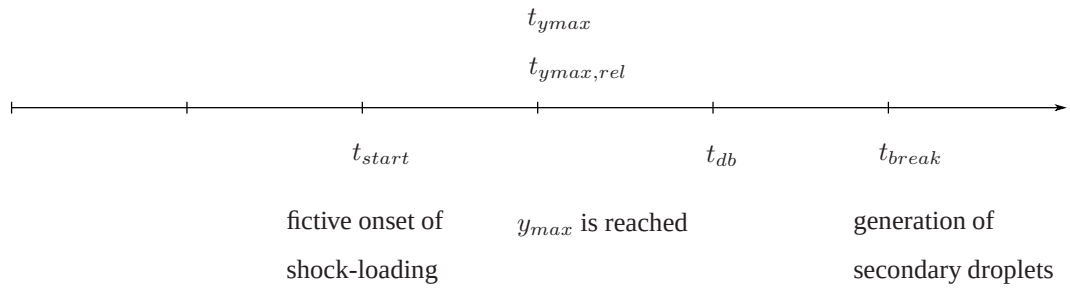

Figure 4. Sequencing schematic of the deformation and breakup process

These values are used for Ohnesorge numbers On < 1. For On > 1, the following correlation for the breakup time as suggested by Willmann [31] is used:

$$\frac{t_b}{t_0^*} = 4.5\left(1 + 1.2\,On^{0.74}\right) . \tag{9}$$

The correlation for the breakup time proposed by Pilch and Erdman [21] is plotted in Figure 2. Since this correlation poorly agrees with the end of breakup times obtained by Dai and Faeth [4], the use of the breakup times reported by Dai and Faeth [4] will be examined in future work.

Representative secondary droplets are created by the model at a discrete breakup time t_{break}. For the bag and multimode breakup regime, most of the initial droplet volume is fragmented during the breakup of the ring and plume/core droplet complex, which occurs at later stages, as illustrated in Figure 2. Therefore, t_{break} is assumed to be uniformly distributed across the second half of the initiation time $t_i = 1.6\,t_0^*$ and t_b. The tracking of a minimum amount of representative droplets ensures an equal distribution of the temporal release of the fragments. Because sheet thinning occurs continuously, t_{break} is assumed to be uniformly distributed between t_i and t_b in the sheet thinning regime.

Global atomization products

The fragment properties resulting from secondary atomization can be described globally, as proposed by Schmehl et al. [24]. The Sauter mean diameter D_{32} of the droplet fragments is obtained from:

$$\frac{D_{32}}{D_0} = 1.5\ \mathrm{On}^{0.2}\ \mathrm{We}_{corr}^{-0.25} , \tag{10}$$

where $\mathrm{We}_{corr} = \mathrm{We}/\left(1 + 1.077\mathrm{On}^{1.6}\right)$. The mass median diameter and the Sauter mean diameter of root normal distributions are related by $D_{0.5}/D_{32} = 1.2$. The secondary droplet sizes D_{sec} are then generated using a root normal distribution [28]

$$f(x) = \frac{1}{2\,\sigma\sqrt{2\,\pi\,x}} exp\left[-\frac{1}{2}\left[\frac{\sqrt{x}-\mu}{\sigma}\right]^2\right] \tag{11}$$

with the parameters $x = D_{sec}/D_{0.5}$, $\mu = 1$ and $\sigma = 0.238$. A reduced Sauter mean diameter is used in the plume-sheet thinning and sheet thinning breakup regime, taking into account the remaining volume of the core droplet. The secondary droplets are generated at a discrete time t_{break} and inherit the velocity of the parent droplet. According to Schmehl et al. [26], only large droplets require a specification of the transverse velocity, since small fragments adopt quickly the gas flow velocity. In bag and multimode breakup (excluding the stamen), these droplets are subjected to an additional transverse velocity component $v_t = \left(D_{r,max} - D_0\right)/2\left(t_b - t_i\right)$, with $D_{r,max}$ being the maximum diameter of the rim column. This transverse velocity is based on the mean velocity of the rim expansion. The volume flow rate is split equally to every tracked representative secondary droplet.

Detailed atomization products

This section describes a detailed modeling of droplet breakup products. The modeling is based on experimental data obtained in shock-tube facilities and published by Chou and Faeth [2, 3] and Dai and Faeth [4]. Chryssakis and Assanis [5] based their unified fuel spray breakup model for internal combustion engines on the same experimental data, however here the implementation differs.

Dai and Faeth [4] studied the breakup for $15 < \mathrm{We}_0 < 150$, $\rho_d/\rho_g > 500$ and $\mathrm{On} < 0.1$. Pulsed shadowgraphy and holography were used to observe the breakup evolution and products in a shock tube. The ratio of the volume fraction of the droplet fragments, V, to the initial droplet volume, V_0, as well as the Sauter mean diameter, D_{32}, normalized by the initial droplet diameter, D_0, are illustrated in Figure 5.

In the proposed model, secondary droplets are simulated as representative droplets (parcels) which represent a specific volume fraction of the original drop. For $\mathrm{We}_0 < 15$ the diameters and volume fractions reported for $\mathrm{We}_0 = 15$ are used. For $15 < \mathrm{We}_0 < 50$, the diameter ratios and volume fractions are linearly interpolated between the documented experimental values. For $\mathrm{We} > 50$, only the core droplet remains and its secondary droplets are generated according to the following proposed treatment for the sheet thinning mechanism. The drop

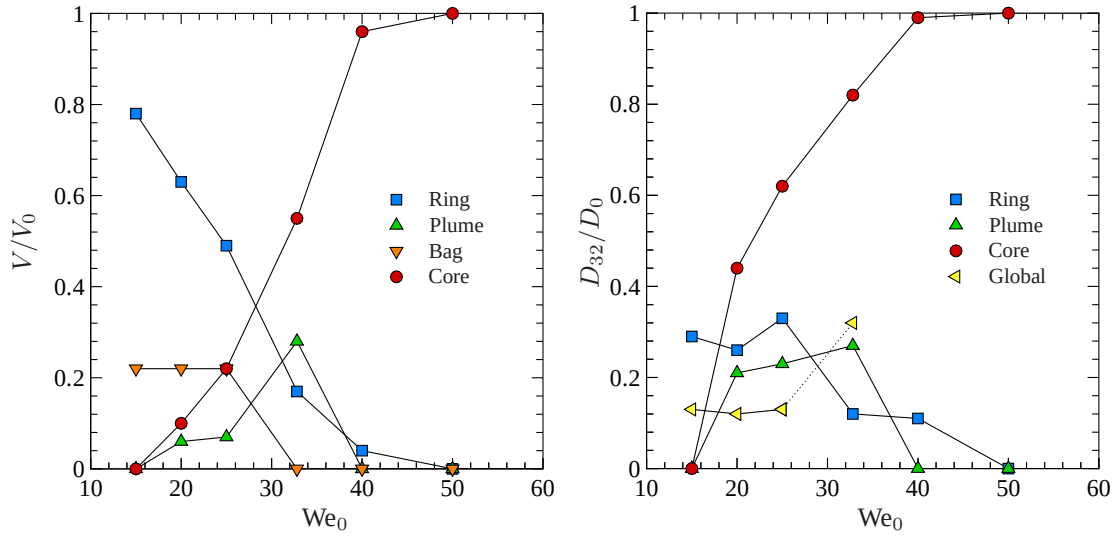

Figure 5. Volume fraction (left) and Sauter mean diameter (right). Experimental data from [4], Figure adopted from [26].

group diameters should be treated as being approximately monodisperse, according to Dai and Faeth [4].

According to Chou and Faeth [3], the basal ring during bag breakup disintegrates due to a Rayleigh-like breakup process (capillary instability), which creates larger node drops and smaller ring drops. In the study of Dai and Faeth [4] ring and node drops of the basal ring are not discriminated and the volume of both groups is combined in the ring drop volume. At $15 < \mathrm{We}_0 < 17$, a ratio of the mean node drop to the mean ring drop diameter of $D_{node} = 1.448\, D_{ring}$ can be derived from [3]. The reported ring volume by Dai and Faeth [4] is split into 46% for the node drops, and 54% for the ring drops. Since no experimental data about the evolution of the distribution of the node and ring volume with We_0 is known, the mentioned volume fraction for the ring and node droplets as well as the mean node drop size D_{node} are assumed for $15 < \mathrm{We} < 32.8$.

Eggers [6] reports in detail about the the formation of main and satellite droplets due to capillary breakup. Future work will investigate if the node drops could be viewed as main drops and the ring drops as satellite drops resulting from capillary breakup of the ring. The breakup time of the ring has some stochastic fluctuations, which leads to different ring diameters at breakup. The distribution of node drops of the ring and ring drops is not perfectly discrete. Since the ring and plume-core droplet breakup due to capillary instability, the droplet sizes exhibit scatter. Therefore, normal distributions of the ring, plume and core droplet sizes were assumed instead of mono-disperse drop groups. The reported droplet sizes by Dai and Faeth [4] are used as mean values, and RMS values of 10 % are assumed.

Chou and Faeth [3] reported fragment sizes due to breakup of the bag of $D = 0.03 - 0.05\, D_0$. Since these fragment sizes were not resolved in the measurements of Dai and Faeth [4], they reported that the bag drops in the multimode breakup regime were either comparable to or smaller than those measured by Chou and Faeth [3]. Therefore, it is proposed to use these droplet sizes to predict the fragment sizes due to breakup of the bag in the whole range of bag and bag-plume breakup.

For Weber numbers smaller $\mathrm{We}_0 < 40$, the breakup event is assumed at a discrete time t_{break}. For $\mathrm{We}_0 \geq 40$, the core droplet is assumed to breakup by sheet thinning. The overlap of plume breakup and sheet thinning shown in Figure 2 is neglected here. The mass flow rate of the generated secondary droplets are adapted according to the

volume fractions as displayed in Figure 5.

A "quasi-continuous" generation of secondary droplets is proposed for droplet breakup in the sheet thinning breakup regime. Chou et al. [2] propose a continuous mass decrease from the core droplet due to the generation of secondary droplets for $125 < \mathrm{We}_0 < 375$, which can be described by a clipped Gaussian function:

$$\frac{1}{m_{d,0}}\frac{dm_d}{dT} = 0.042\, exp\left[0.8\,(T-3.5)^2\right], \qquad \text{for} \quad 1.5 < T < 5.5 \tag{12}$$

The change in diameter of the core droplet can then be calculated. According to Chou et al. [2], a transient and a quasi-steady shear breakup regime can be observed. They propose the following correlation for the Sauter Mean Diameters of the secondary droplets sizes:

$$\frac{D_{32}}{D_0} = \begin{cases} 2\sqrt{T_\zeta}\,, & \text{for} \quad T_\zeta < 0.002 \\ 0.09\,, & \text{for} \quad T_\zeta > 0.002 \end{cases} \tag{13}$$

with $T_\zeta = \mu_d t/\left(D_0^2 \rho_d\right)$. Chou et al. documented a standard deviation of 22% for the right hand side of Equation (13) for $T_\zeta > 0.002$. Therefore, a normal distribution of the secondary droplet sizes with the mean diameter according to Equation (13) and a RMS value of 22% is proposed. The transient shear breakup regime will not be resolved in many applications, since the onset of the modeled breakup process often starts later than $T_\zeta = 0.002$. The generation of secondary droplets is implemented as a linear function of time. To achieve mass closure, the reduction of the core droplet mass flow is transfered to the secondary droplets.

In the bag and multimode breakup regime, the generated droplets inherit the velocity of the parent drop. The ring and node drops created during bag breakup inherit additionally the momentum of the expanding liquid ring. For this, the transversal velocity is derived from Equation (5) to be $v_t/v^* = dy/dT = 3.2$, with the characteristic velocity $v^* = v_{rel}\,(\rho_g/\rho_d)^{0.5}$. The fragments of the stamen breakup result from capillary breakup which does not add a significant momentum. Since the fragments resulting of bag breakup are small, no additional velocity component needs to be specified. These drop groups inherit therefore no additional velocity component.

In the sheet-thinning regime, the mean transverse velocity of the secondary droplets is approximately zero, but the fragments are accelerated in the streamwise direction, according to Chou and Faeth [2]. They report following relation for the mean streamwise velocity:

$$\bar{v}_z = 9.5\, v^* + v_d \tag{14}$$

with the velocity of the parent drop v_d. The RMS velocities in streamwise and transverse direction result in $\bar{v'}_z/v_{rel} = 0.2$ and $\bar{v'}_t/v_{rel} = 0.23$.

Open issues to be addressed

Future work will focus on the proper determination of RMS-values of the secondary droplet sizes. The modeling of the breakup of the core droplet in plume-shear breakup should be improved. The onset of sheet thinning and the mass reduction has to be adapted for $\mathrm{We}_0 < 125$. The influence of the Ohnesorge number has to be assessed. The use of Equation (12) needs a minimum amount of representative secondary droplets to be tracked, otherwise too much mass would be removed close to $T = 1.5$ and $T = 5.5$. Chryssakis and Assanis [5] modeled the mass decrease of the core droplet with a boundary layer stripping approach, which assumes a constant mass decrease in time. It will be investigated, if this approach can be used for simulations with fewer parcels which are to be tracked. The implementation of the recovery of a droplet whose aerodynamic loading changed to a subcritical loading during the breakup process is planned.

Comparison of droplet size distributions

In this section, the presented global statistical and detailed fragment size model are compared. Droplets at shock-loading conditions have been placed in a constant gas flow at Weber numbers $\mathrm{We}_0 = 15, 25, 70$ and 125. Laminar flow is assumed, so no stochastic deviations of the gas phase exist. Ten thousand parcels have been injected, with 5 generated parcels per breakup event for bag and bag-plume breakup, and 20 generated parcels per breakup event for plume-sheet-thinning and sheet-thinning breakup. Droplet deformation is calculated with the NLTAB model. The inhouse particle tracking code Ladrop is used in this study. The cumulative sum curve is compared to data obtained by Hsiang and Faeth [11] and Chou and Faeth [3].

Figures 6a and 6b depict the cumulative volume sum for $\mathrm{We}_0 = 15$ and $\mathrm{We}_0 = 25$. The volume fraction of the secondary droplets is displayed as a function of the ratio of the secondary droplet size to the mass median diameter, $x = D/D_{0.5}$.

The predicted cumulative volume sums using the global atomization approach fit well to the experimental data for bag and bag-plume breakup (Figures 6a,6b). Predictions using the detailed fragment size model yield a volume fraction of 22% for the small fragments resulting of the breakup of the bag. A discrimination of the ring and node droplets can be observed. In the bag-plume breakup regime, the droplet group of the plume is also modeled. The cumulative volume sum predicted by the detailed breakup product model lies within the scatter of experimental results, with the exception of the droplets resulting by the fragmentation of the bag. Kombayasi et al. [14] and Gelfand et al. [7] report a bimodal size distribution for the droplets generated by the bag breakup mechanism. According to Chou and Faeth [3], Hsiang and Faeth [11] underrepresented the droplets generated by the bag during bag breakup. In the study of Chou and Faeth [3], the small droplets resulting from the disintegration of the bag tend to be undersampled since they are small and accelerate rapidly to the gas velocity. No further detailed studies on bag and bag-plume breakup are known to exist [9].

The cumulative volume sums for $We_0 = 70$ and $We_0 = 125$ are plotted in Figures 6c and 6d. The cumulative volume sums stagnate at about 80%, and the remaining 20% of the volume belong to the core droplet. Both approaches yield droplet distributions which fit to the experimental data. Since the transient phase of the sheet thinning mechanism according to Equation (13) is not captured, the smaller droplet sizes described by the sheet thinning mechanism are not predicted by the detailed model, which results in a narrower droplet size distribution. A comparison of both models with a validation test case is needed to draw a final conclusion.

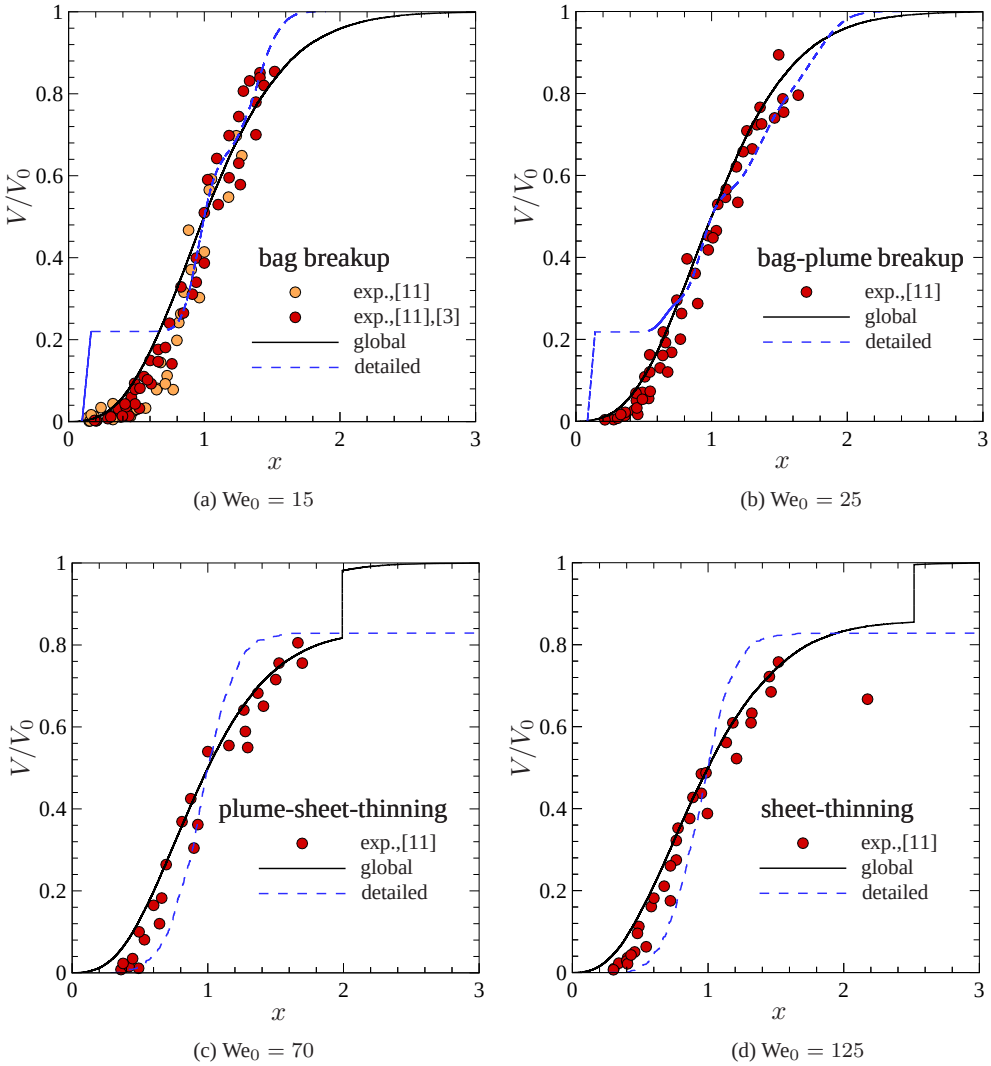

(a) $We_0 = 15$ (b) $We_0 = 25$

(c) $We_0 = 70$ (d) $We_0 = 125$

Figure 6. Comparison of droplet size distributions

Injection of a droplet in a gas cross-flow

The aim of this test case is the comparison of breakup models with a deformation-based breakup criteria to models with a criteria based on the local instantaneous Weber number. Therefore, the proposed model by Schmehl et al. [24], in the following referred to as semi-empirical model, is compared to the breakup model proposed in this paper, with a discrimination of global statistical and detailed secondary droplet modeling, which are referred to as deformation-based model with global or detailed atomization products.

The test case is an injection of a droplet chain into a gas cross-flow, which Park et al. [20] investigated experimentally. They measured the secondary droplet sizes for We $= 68$, 153, and 383 with Phase Doppler Anemometry. They injected diesel drops with a mono-disperse diameter of $184\ \mu m$ into a gas cross flow at ambient conditions ($p = 10^5\ Pa$, $T = 293\ K$). The droplet velocity was measured to be $13.4\ m/s$ at the center of the gas jet axis without gas issuing. The distance between the injected droplet centers was about twice their diameter, therefore the influence of droplet wakes may be important.

The flowfield of the gas phase has been calculated with the incompressible, steady-state solver simpleFoam, which is part of OpenFOAM-1.6.x. The axially symmetric mesh consists of 576080 cells. Gas phase turbulence is resolved by the $k - \varepsilon$-model. Since Park et al. [20] did not give details about the gas phase, a turbulence level of 5 % has been assumed at the inlet. It is also assumed, that the reference Weber number is calculated with the maximum gas phase velocity. The setup for the test case is shown in Figure 7 (left).

The dispersed phase has been predicted with the inhouse code Ladrop. Five thousand representative diesel droplets with an initial diameter of $184\ \mu m$ have been injected at a location of x,y,z=$(-0.02, 0, 0)m$ with an initial velocity of $14.6\ m/s$ in x-direction. Turbulent dispersion of the dispersed liquid phase has been accounted for by the model of Gosman and Ioannides [8]. Droplet deformation has been computed by the NLTAB-model. In this case, only coupling of the gas-phase to the dispersed phase (one-way-coupling) was accounted for as a first estimate.

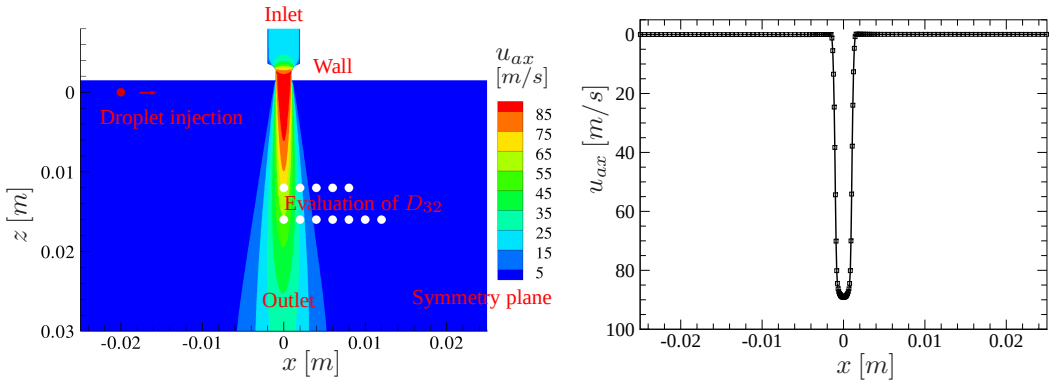

Figure 7. Setup of the test case (left), gas phase velocity at $y = 0$ and $z = 0$ (right)

The axial velocity profile of the gasphase at the axial distance of droplet injection is depicted in Figure 7 (right). It can be seen that the aerodynamic loading varies significantly as the droplet crosses the gas jet. Predicted trajectories are displayed in Figures 8a to 8c and Figure 8d shows an experimental visualization of the spray. The initial deflection of the predicted trajectories can be compared to the microscopic visualizations. It can be concluded, that the proposed models which resolve the deformation during the breakup process predict the initial deformation phase well. The continuous stripping of droplets as predicted by the detailed atomization model can be observed in Figure 8c, which enhances the dispersion of small droplets. The semi-empirical model uses the instantaneous Weber and Ohnesorge number when the critical Weber number is first exceeded for the calculation of characteristic times and diameters. Therefore, the calculation of the characteristic deformation time is based on a comparatively low Weber number and the resulting breakup period is overestimated. Consequently, the generation of secondary droplets occurs when the droplets have almost left the gas jet and results to significant errors of the predicted droplet trajectories.

The overall spray angle of the calculated trajectories can be compared to the apparent spray angle, depicted in the macroscopic images. The deformation-based breakup models predict well the spray angle in contrast to the

semi-empirical model. The Sauter mean diameters at three different axial positions are plotted in Figure 9. The

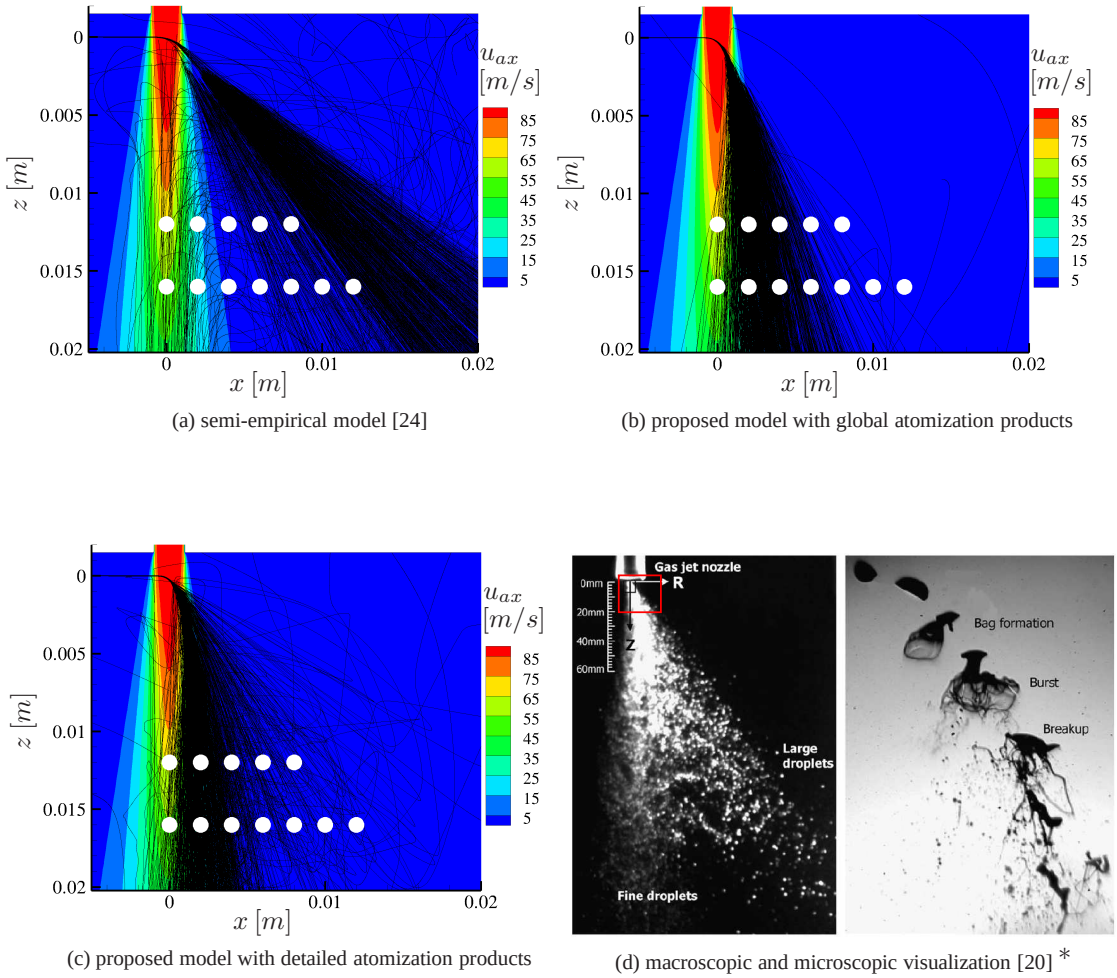

(a) semi-empirical model [24]

(b) proposed model with global atomization products

(c) proposed model with detailed atomization products

(d) macroscopic and microscopic visualization [20] *

Figure 8. Comparison of computed and measured trajectories

semi-empirical model predicts only a few trajectories which pass through the plane, where D_{32} is evaluated, as can be seen in Figure 8a. The Sauter mean diameters predicted by the global atomization model are in good agreement with the measured ones close to the centerline. Deviations of the predicted and measured D_{32} can be attributed to the low density of parcels at larger radial distances. It should be noted, that the Weber number of We $= 68$ led to a plume-sheet-thinning breakup regime, whereas in the microscopic visualizations of Park et al. [20] a more complex bag-plume breakup regime can be observed.

Therefore, detailed experimental investigations are necessary to assess the influence of the modeling of secondary atomization products. In such an investigation, precise knowledge of the gas phase boundary conditions is necessary. Furthermore, droplets should be injected at lower rates to obtain negligible influence of droplet wakes and to be able to neglect the influence of the dispersed phase on the air flow. Also, a distribution of the liquid volume flux is needed to assess the validity of the statistics. Finally, if large droplets are injected, the possibility of a rotational momentum due to the different velocity loading on both hemispheres has to be taken into account. No detailed statement can therefore be given as to the validity of the effect of atomization product modeling. It can be concluded, that the proposed deformation based models predict well the overall trajectories and deformation during the breakup process.

*Reprinted from International Journal of Multiphase Flow, Volume 32(7), S. W. Park, S. Kim and C. S. Lee, Breakup and characteristics of mono-dispersed diesel droplets in a cross-flow air stream, pp. 807-822, 2006, with permission from Elsevier.

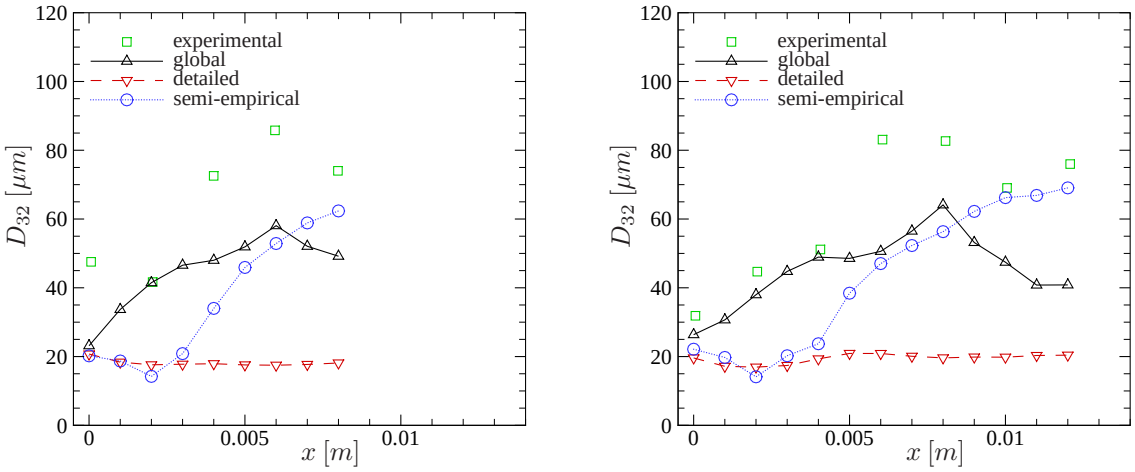

Figure 9. Comparison of SMD, $z = 12mm$ (left) and $z = 16mm$ (right). Experimental data from [20].

Conclusions

A breakup model has been proposed, with a breakup criterion based on the critical deformation. The NLTAB-model is used to resolve droplet deformation until a specified deformation is reached. Different breakup regimes are identified using the Weber number when the droplet deformation reaches the critical deformation. Following this, droplet deformation during breakup is predicted by empirical correlations. Since the aerodynamic loading of the droplet does not typically correspond to shock-loading, correlations based on the NLTAB-model have been proposed to predict the fictive Weber number and characteristic non-dimensional time for shock-loading conditions. In addition, a model for detailed secondary atomization products is proposed, which differentiates between the bag, bag-plume, plume-sheet-thinning and sheet-thinning regime.

Cumulative volume sums have been predicted by the proposed detailed atomization product model and a global statistical atomization product model presented by Schmehl et al. [24]. Good agreement with experimental data is observed in both cases. The detailed atomization product model accounts for the volume fraction of the fine droplets produced by the fragmentation of the bag during bag and bag-plume breakup. Since this droplet group can represent up to 22% of the initial droplet volume, predictions using the detailed breakup product model should enhance the accurate determination of droplet evaporation.

Droplet trajectories and diameters have been compared with an experimental test case, an injection of a diesel droplet chain into a cross-flow. The deformation-based breakup models proposed in this paper adequately predict the deformation during the breakup process as well as the overall cone angle. This is in contrast to previous models, such as the semi-empirical model [24], which predict characteristic times using an instantaneous Weber number at the time step when the critical Weber number is first exceeded. In the presented test case, this Weber number is significantly lower than the maximum Weber number in the gas jet. Consequently, characteristic times are overestimated, resulting in significant disagreement between experimentally obtained and predicted secondary droplet trajectories.

The accuracy of the detailed atomization model could not be validated due to the lack of experimental data. Further detailed experimental research including documentation of boundary conditions of the liquid and gas phase is needed.

Acknowledgments

The work described within this paper was mainly supported and funded by the German Federal Department of Economy and Labour under contract 20T0602 ("GerMaTec") as part of the German national aeronautical research programme. The support is gratefully acknowledged. The authors thank Daniel R. Guildenbecher for valuable comments.

Nomenclature

A_c	acceleration parameter [-]
D	cross stream diameter [m]
D_{32}	Sauter mean diameter [m]
E	aspect ratio [-]
N	number [-]
T	non-dimensional time [-]
T	temperature [K]
c_D	drag coefficient [-]
m	mass [kg]
p	pressure [Pa]
t	time [s]
v	velocity [m·s^{-1}]
y	non-dimensional equator coordinate [-]
μ	dynamic viscosity [Pa·s]
μ	mean [-]
ρ	density [kg·s^{-3}]
σ	surface tension [N·m^{-1}]
σ	standard deviation [-]

Characteristic numbers

On	$= \mu_d/\sqrt{\rho_d D_0 \sigma}$	Ohnesorge number
Re	$= \rho_g v_{rel} D/\mu_g$	Reynolds number
We	$= \rho_g v_{rel}^2 D_0/\sigma$	Weber number

Subscripts

b	end of breakup
c	critical
d	disperse phase
g	gas
i	initiation
l	liquid
r	ring
t	transverse
break	generation of secondary droplets
corr	corrected
db	disc bulging
max	maximum
rel	relative
start	calculated shock-loading state
y,max	value at maximal non-dimensional coordinate
0	initial

Superscripts

*	characteristic

References

[1] Aalburg, C., van Leer, B. and Faeth, G.M., *AIAA-Journal* 41(12):2371-2378 (2003).
[2] Chou, W.-H., Hsiang, L.-P. and Faeth, G.M., *International Journal of Multiphase Flow* 23(4):651-669 (1997).
[3] Chou, W.-H. and Faeth, G.M., *International Journal of Multiphase Flow* 24(6):889-912 (1998).
[4] Dai, Z. and Faeth, G.M., *International Journal of Multiphase Flow* 27(2):217-236 (2001).
[5] Chryssakis, C. and Assanis, D. N., *Atomization and Sprays* 18(1):1-52 (2008).
[6] Eggers, J., *Reviews of Modern Physics* 69(3):865-929 (1997).
[7] Gel'fand, B. E., Gubin, S. A. and Kogarko, S. M., *Inzhenerno-Fizicheskii Zhurnal* 27(1):119-126 (1974).
[8] Gosman, A. D. and Ioannides, E., *Journal of Energy* 7(6):482-490 (1983).
[9] Guildenbecher, D. R., López-Rivera, C. and Sojka, P. E., *Experiments in Fluids* 46(3):371-402 (2009).

[10] Gutknecht, R., M.Sc. Thesis, Institut für Thermische Strömungsmaschinen, Universität Karlsruhe, 1996.
[11] Hsiang, L.-P. and Faeth, G.M., *International Journal of Multiphase Flow* 18(5):635-652 (1992).
[12] Hsiang, L.-P. and Faeth, G.M., *International Journal of Multiphase Flow* 21(4):545-560 (1995).
[13] Kim, S.S., Ph.D. Thesis, Rutgers University, New Jersey, 1977.
[14] Komabayasi, M., Gonda, T. and Isono, K., *Journal of the Meteorological Society, Japan* 42:330-340 (1964).
[15] Krzeczkowski, S.A., *International Journal of Multiphase Flow* 6:227-239 (1980).
[16] Lane, W. R., *Industry and Engineering Chemistry* 43:1312-1317 (1951).
[17] Leppinen, D.M., Renksizbulut, M. and Haywood, R.J., *Chemical Engineering Science* 51(3):491-501 (1996).
[18] Liu, Z. and Reitz, R. D., *International Journal of Multiphase Flow* 23(4):631-650 (1997).
[19] O'Rourke, P.-J., and Amsden, A.A., *SAE Technical Paper 872089* (1987).
[20] Park, S. W., Kim, S. and Lee, C. S., *International Journal of Multiphase Flow* 32(7):807-822 (2006).
[21] Pilch, M. and Erdman, C.A., *International Journal of Multiphase Flow* 13(6):741-757 (1987).
[22] Reitz, R.D. and Diwakar,R., *SAE Technical Paper 860469* (1986).
[23] Reitz, R.D, *Atomization and Spray Technology* 3:309-337 (1987).
[24] Schmehl, R., Maier, G. and Wittig, S., *Eighth International Conference on Liquid Atomization and Spray Systems*, Pasadena, CA, USA, July 2000, pp. 918-925.
[25] Schmehl, R., *18th Annual Conference on Liquid Atomization and Spray Systems*, Zaragoza, Spain, September 2002, pp. 495-501.
[26] Schmehl, R., Ph.D. Thesis, Institut für Thermische Strömungsmaschinen, Universität Karlsruhe, Germany, 2004. Available from http://digbib.ubka.uni-karlsruhe.de/volltexte/1000018104 .
[27] Schmehl, R. and Steelant, J., *Journal of Propulsion and Power* 25(3): 771-782 (2009).
[28] Simmons, H.C., *ASME-Journal of Engineering for Power* 99:309-314 (1977).
[29] Tanner, F.X., *Journal of Engines*, 106(3):127-140 (1998).
[30] Wierzba, A., *Experiments in Fluids* 9:59-64 (1990).
[31] Willmann, M., Ph.D.Thesis, Institut für Thermische Strömungsmaschinen, Universität Karlsruhe, Germany, 1999.